Chapter-4

4 Biogenic Synthesis of Gold Nanoparticles Using Dual Extract of Tulsi-Vinca for Breast Cancer Tumor Regression in Mice

4.1 Introduction

4.1.1 Threat about Triple-Negative Breast Cancer (TNBC)

Triple-negative breast cancer (TNBC) is immensely heterogenic due to its aggressive clinical phenotype defined by negative profile of estrogen (ER), progesterone (PR) and human epidermal growth factor-2 (HER-2) receptor[204]. However, the current approaches based on ER and HER-2 targeted therapies are still unmet for treating TNBC. In addition, TNBC patients have a high risk of recurrence, metastasis and poor survival rates than patients with other sub-types of breast cancer. Various distinct entities with different biological and clinical behaviours are inadequate for the growth of molecular based targeted therapies. The conventional methods of treatment for TNBC include radio-therapy, multiple chemotherapies cocktail, and surgery associated with acute side effects, late recovery, recurrence, therapy-induced cancers and offer lower selectivity for TNBC population[205]. However, the most common chemotherapeutic regimens derived from plants used – anti-mitotic derived from plants includes paclitaxel, paclitaxel, docetaxel, irinotecan, topotecan, teniposide, etoposide, vinblastine, vincristine and other alkylating agents- carmustine, busulfan, cisplatin, carboplatin. Since, then other antibiotics-Mitomycin C, Cyclophosphamide and Actinomycin-D are associated with cancer suffers from various side effects, non-specificity and drug resistance[206].

4.1.2 Treatment of TNBC

To addressed this, nanotechnology emerged as a promising candidate for the detection and treatment of TNBC. One of the key advantages of nanotechnology is the ability to target and deliver therapeutic agents directly to cancer cells, while minimizing side effects on healthy

tissues[207]. Various studies showed that drug free, metallic nanoparticles gold, silver, iron or gadolinium, exhibited unique features in detecting breast cancer including imaging[208], biosensors[209], liquid biopsy[210], and drug delivery[211]. Green synthesis of nanoparticles offers a safe, sustainable, environment friendly, and cost-effective than other modes of synthesis. Among metallic NPs, gold NPs have immersive biomedical relevance, due to their anti-microbial, anti-cancer, anti-inflammatory and anti-oxidant activities without prior off-target toxicity and immunogenicity. Additionally, the small size and high surface area of nanoparticles enables them to interact with cells and exploited for targeted drug delivery and imaging system[212].

4.1.3 Meditational properties of Tulsi and Vinca

Tulsi (*Ocimum sanctum)* and *Vinca* (*Vinca minor*) plant leaves are used as reducing agents, for the synthesis of gold nanoparticles due to their inherent phytochemical properties[213], [214]. Eugenol, a major component of Tulsi oils has been exhibited anti-inflammatory and antioxidant properties[215]. Rosmarinic acid has been reported to exhibit anti-cancer effects through the modulation of various signalling pathways[216]. Tulsi contains the flavonoid apigenin, which has been shown to inhibit cell proliferation and induce apoptosis in cancer cells[217]. Furthermore, clinical data of *Vinca* contains alkaloids like vincristine and vinblastine that are reported to treated leukaemia and lymphoma[218], [219] by hijacking the growth and completely regressing the cancer proliferation[219]. Emerging evidence suggests that Tulsi extracts can trigger the immune cells and help regulate various infections, allergies, and autoimmune disorders[220]. Additionally, Tulsi has been traditionally used as an adaptogen, which can help the body to adapt stress[221]. *Vinca* extracts have also been reported to have anti-diabetic, anti-oxidant, and anti-inflammatory effects[222]. A plethora of literature suggest that gold nanoparticles derived from Tulsi and *Vinca* leaf extract exhibit remarkable stability

and biocompatibility in cancer management by specifically targeting the cancer and inducing apoptosis[223], [224]. Although these studies encourage the ability for ample clinical use of mixed extracts of green AuNPs for cancer treatment, AuNPs are pleotropic stressors, and it is necessary to scrutinize sub- lethal, off-target toxicity which could provide the route for their safety and clinical translation.

In this study, we determine the hypothesis that an TNBC may be vulnerable to exploitable green gold nanoparticles (GNPs), and evaluate the how the GNPs derived from mixed extract of Tulsi and *Vinca* leaves, affects the sensitivity of TNBC cells to GNPs. The nanoparticles were also evaluated for their free radical scavenging activity and cytotoxicity using GNPs. The T-Gold and V-Gold nanoparticles were used as individuals controls for comparison with T+V-Gold. The T+V-Gold nanoparticles showed a higher degree of stability and biocompatibility than T-Gold and V-Gold. To determine potential off-target, sub-lethal effects of GNPs, we measure the cytotoxic effect of GNPs and their composite against 4T1 cells. Furthermore, *in vivo* studies were performed to evaluate the efficacy, tolerability and ROS level of interperitoneally administered GNPs for treatment of 4T1 induced TNBC murine model. These studies help to build link cell culture to murine TNBC model and further human studies will provide future advancements of GNPs for treatment of TNBC and their clinical usage.

4.2 Results

4.2.1 Characterization of GNPs

A transmission electron microscopy (TEM) image of gold nanoparticles (GNPs) produced using extracts of Tulsi, *Vinca*, and a 1:1 mixture of Tulsi and *Vinca* showed the presence of particles with diverse shapes and sizes (Figure 4.1(a-c)). The particle sizes ranged from approximately 10 nm to 250 nm, with the smaller particles having a spherical or semi-spherical

shape. In contrast, the larger particles exhibited triangular, pentagonal, and hexagonal geometries. Such geometric variations have been previously reported in the literature[225]–[228]. The absorption spectra of T-Gold, V-Gold, and T+V-Gold are displayed in Figure 4.1(d). The spectra exhibited two distinct absorption bands at 285 and 555±15 nm. The weak absorption band observed at 285 nm was attributed to the π - π* transition of the C=O bond[229]. The absorption band observed at 555±15 nm was attributed to the phenomenon of localized surface plasmon resonance (LSPR)[230]. The LSPR arises from the collective oscillations of the conduction electrons in the metal nanoparticles induced by the interaction with incident light. The resultant plasmons generate a strong electromagnetic field, leading to an absorption band in the visible to near-infrared region of the electromagnetic spectrum.

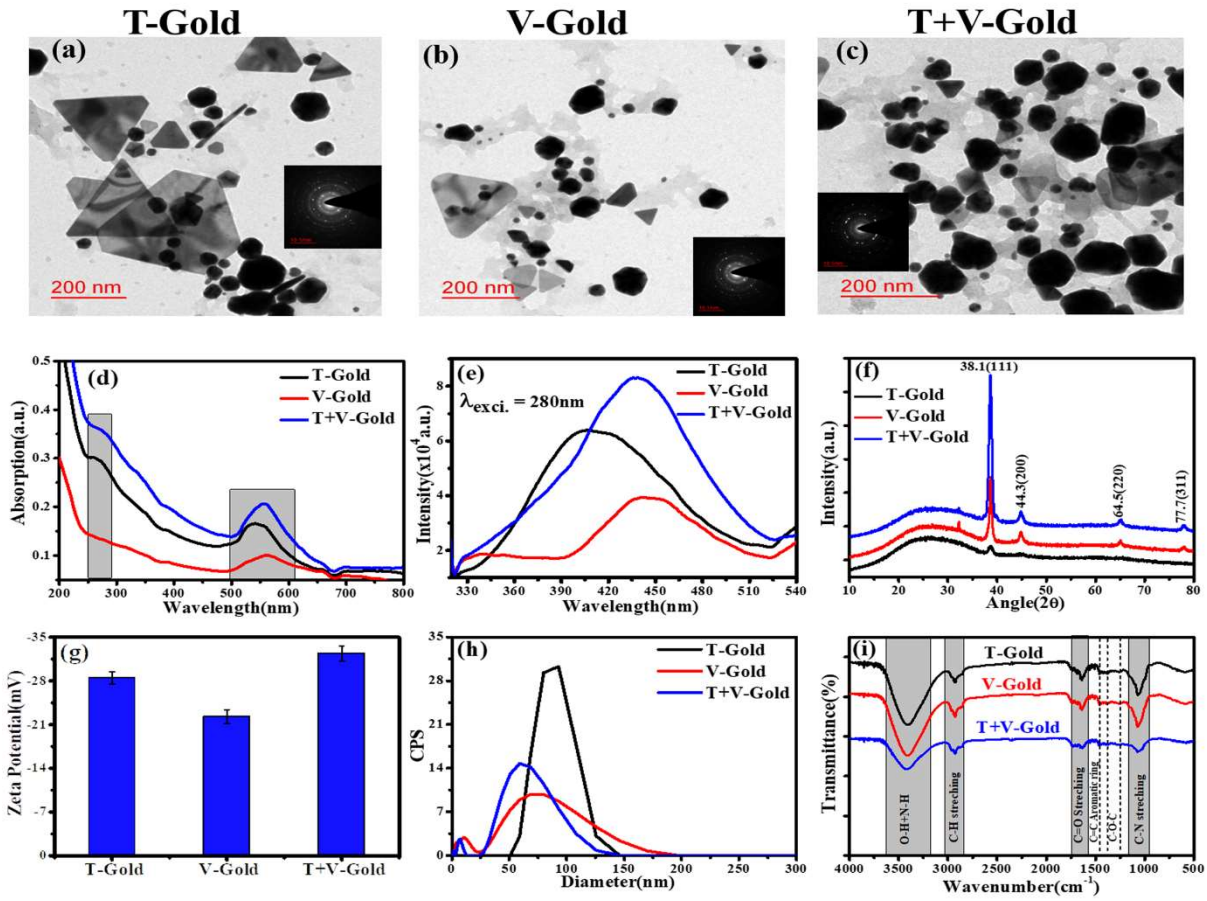

Figure 4. 1 (a), (b), and (c) shows the TEM image, inset (a), (b), and (c) shows the SAED pattern of T-Gold, V-Gold, and T+V-Gold. (d) UV-VIS spectra, (e) Emission spectra at fixed

excitation 280 nm, (f) XRD patterns, (g) Zeta potential and, (h) DLS of T-Gold, V-Gold, and T+V-Gold nanoparticles (i) FTIR Spectra of T-Gold, V-Gold, and T+V-Gold.

The exact position and intensity of the absorption band were influenced by various factors, such as the size, shape, and composition of the nanoparticles, as well as the dielectric environment in which they were situated. The XRD technique was used to investigate the crystallinity of the synthesized gold nanoparticles (GNPs), and the corresponding XRD patterns are presented in Figure 4.1(f). The functionalized GNPs exhibited four distinct peaks at 2Θ = 38.1, 44.3, 64.5, and 77.7, corresponding to the miller indices (111), (200), (220), and (311), respectively indicating a face-centred cubic (FCC) lattice structure[231].The zeta potential of the synthesized samples was measured at 25 $^{\circ}$C, and all the samples exhibited negative zeta potential values within the range of -20 to -35 mV shown in Figure 4.1(g). This range was known to indicate stable colloidal solutions, as reported in previous studies[232], [233].

4.2.2 Fourier-transform infrared (FTIR) and XPS Analysis

The FTIR spectra of T-Gold, V-Gold, and T+V-Gold samples were analysed, and the presence of surface functional groups was observed as shown in Figure 4.1(i). The spectra showed a broad peak at 3417 cm^{-1}, which was indicative of O-H and N-H stretching vibrations, while the C-H stretching vibrations produced a medium, and moderate absorption peak at 2929 cm^{-1}. The carbonyl groups, characterized by C=O stretching modes of vibration, were observed at 1730 cm^{-1}, and the C=C or aromatic ring stretching modes were observed at 1633 cm^{-1}[189]. The C-O-C stretching vibration produced a peak at 1268 cm^{-1}, while the C-N stretching vibration resulted in a peak at 1062 cm^{-1}. The chemical composition of T-Gold, V-Gold, and T+V-Gold samples were analysed using X-ray photoelectron spectroscopy (XPS).

4.2.3 XPS Analysis of GNPs

Survey spectra were obtained by collecting XPS signals over a photon energy range of 0 to 1350 eV, as shown in Figure 4.2(a). The C1s, O1s, and Au 4f photoelectron peaks of each sample were then examined and displayed in Figure 4.2 (b-d), respectively. Notably, we observed significant differences in peak shape, indicating different percentages of functional groups present in the synthesized samples.

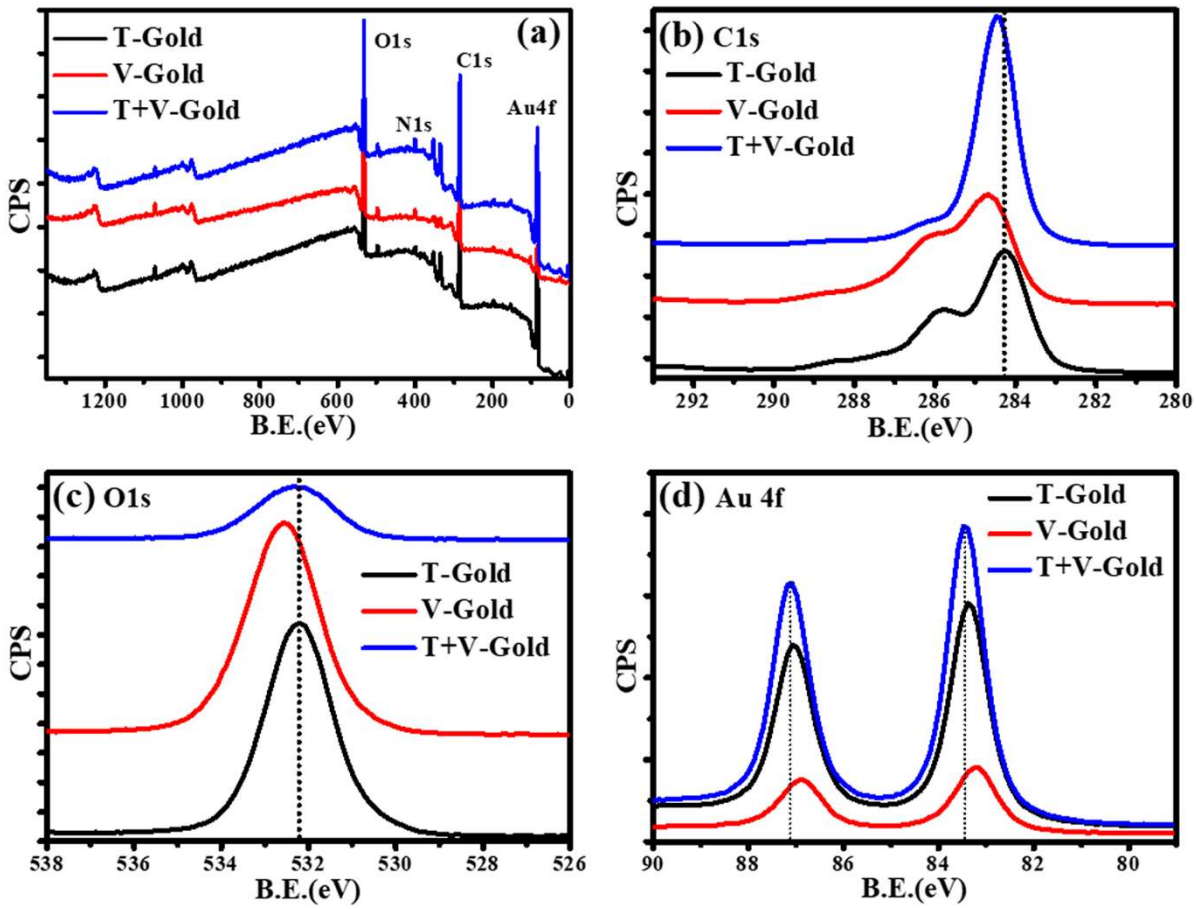

Figure 4. 2 (a) XPS survey spectrum of T-Gold, V-Gold, and T+V-Gold samples, (b) C1s, (c) O1s, (d) Au 4f high resolution XPS photoelectron peaks of T-Gold, V-Gold, and T+V-Gold.

To further investigate these differences, the photoelectron peaks were deconvoluted, as shown in Figure 4.3(a-i). The major component of C1s deconvolution is C=O, C-O/C-N, and C-

C/C=C, while O1s shows the C-O/C=O, O-C=O, and O-O functional groups found and corresponding Au 4f obtained only $4f_{5/2}$ and $4f_{7/2}$ photoelectron deconvolution peaks.

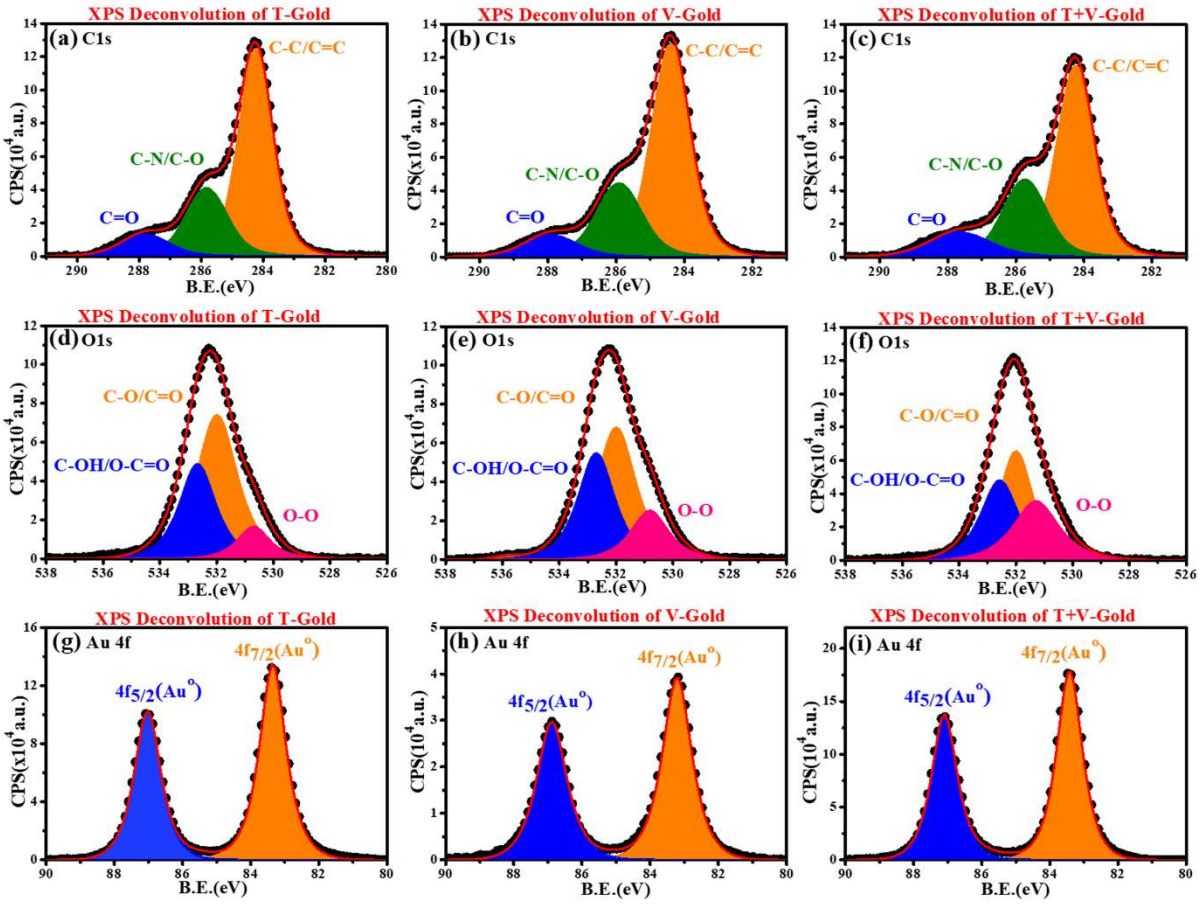

Figure 4. 3 Deconvolution of XPS photoelectron peak spectra. (a) T-Gold, (b) V-Gold, (c) T+V-Gold, deconvolution of C1s XPS spectra, (d) T-Gold, (e) V-Gold, (f) T+V-Gold, deconvolution of O1s XPS spectra, (g) T-Gold, (h) V-Gold, (i) T+V-Gold, deconvolution of Au 4f XPS spectra.

4.2.4 Free Radical Scavenging Analysis

The DPPH radical is known to exhibit maximum absorption at 517 nm, and its reduction can be monitored by the decrease in absorbance at this wavelength upon the addition of antiradical/antioxidant samples. This phenomenon has been widely used to screen antiradical compounds, as it provides a simple, precise, and cost-effective method for evaluating their activity (Figure 4.4(a), (d), and (g)). Additionally, the accuracy and precision of the method

allows for reliable and reproducible results to be obtained, which was crucial for evaluating the activity of different antiradical compounds[234].

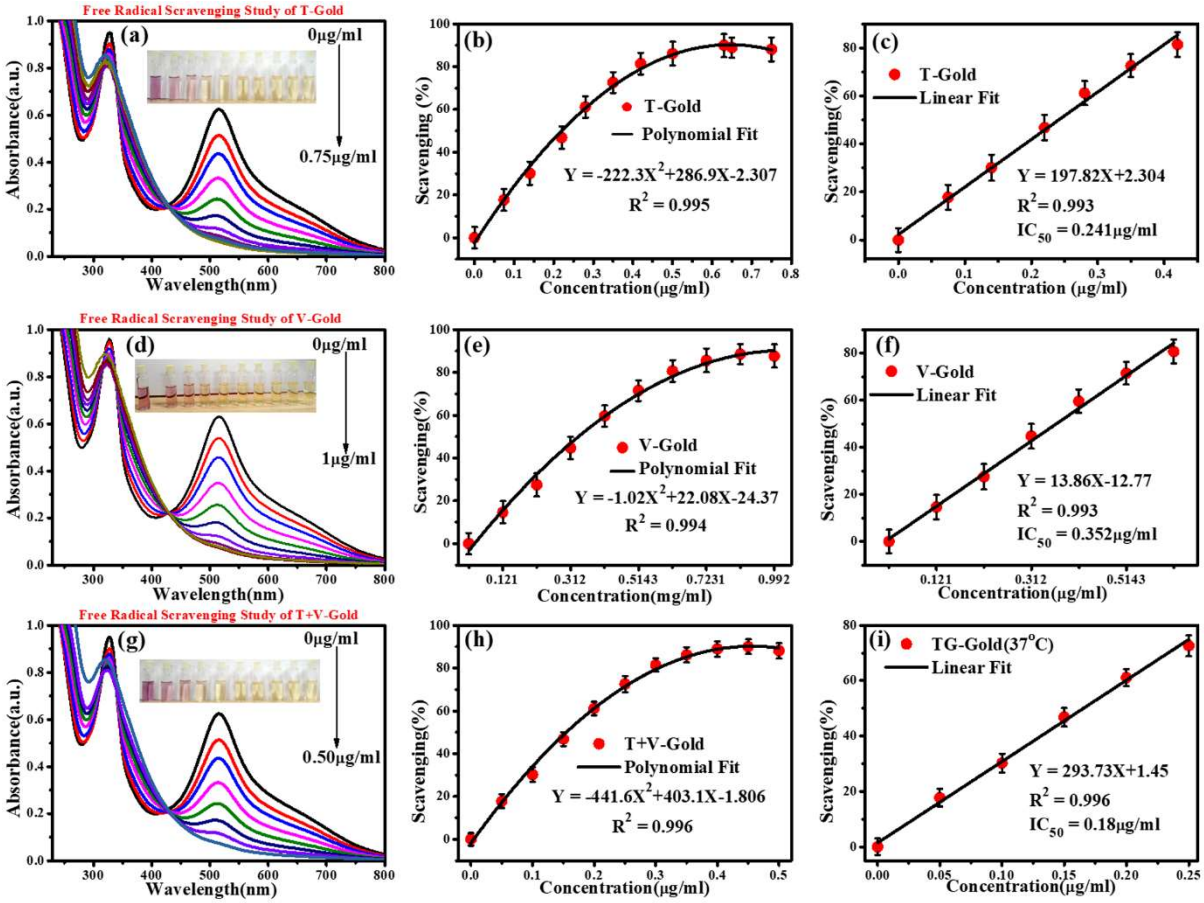

Figure 4. 4 DPPH radical scavenging assay of T-Gold, V-Gold, and T+V-Gold. (a) T-Gold, (d) V-Gold, (g) T+V-Gold UV-VIS absorption spectra of DPPH radical upon a gradual increase of T-Gold, V-Gold, and T+V-Gold, inset shows the photograph of DPPH solution exposed with different concentration of T-Gold, V-Gold, and T+V-Gold. (b), (e), and (h) shows the calibration curve of percentage scavenging of DPPH radicals vs different concentration of T-Gold, V-Gold, and T+V-Gold. (c), (f), (i) shows the linear range of scavenging percentage vs different concentration of T-Gold, V-Gold, and T+V-Gold and calculate the IC_{50} value.

Overall, the DPPH assay method provides a valuable tool for screening the antioxidant activity of different samples, including T-Gold, V-Gold, and T+V-Gold in this study. The use of this

method can facilitate the identification of potential antioxidant compounds, which can have significant implications in various fields, including medicine, food, and cosmetics.

4.2.5 *in vitro* Cytotoxicity Studies

In in-vitro studies, significant cytotoxicity was observed starting at 50 µg/ml to 200 µg/ml for T-Gold, V-Gold and T+V-Gold, formulation resulted in a dose-dependent manner to inhibit the growth of NIH- 3T3 cells (Figure 4.5(d-f)). Furthermore, the effects of T-Gold, V-Gold and T+V-Gold were evaluated separately over a period of 3 days (72 hours) in real-time, and the IC_{50} values were calculated at different time points. The IC_{50} values of T-Gold, V-Gold and T+V-Gold depleted over the time, suggesting time-dependent cytotoxicity against 4T1 metastatic breast cancer (Figure 4.5(a-c)).

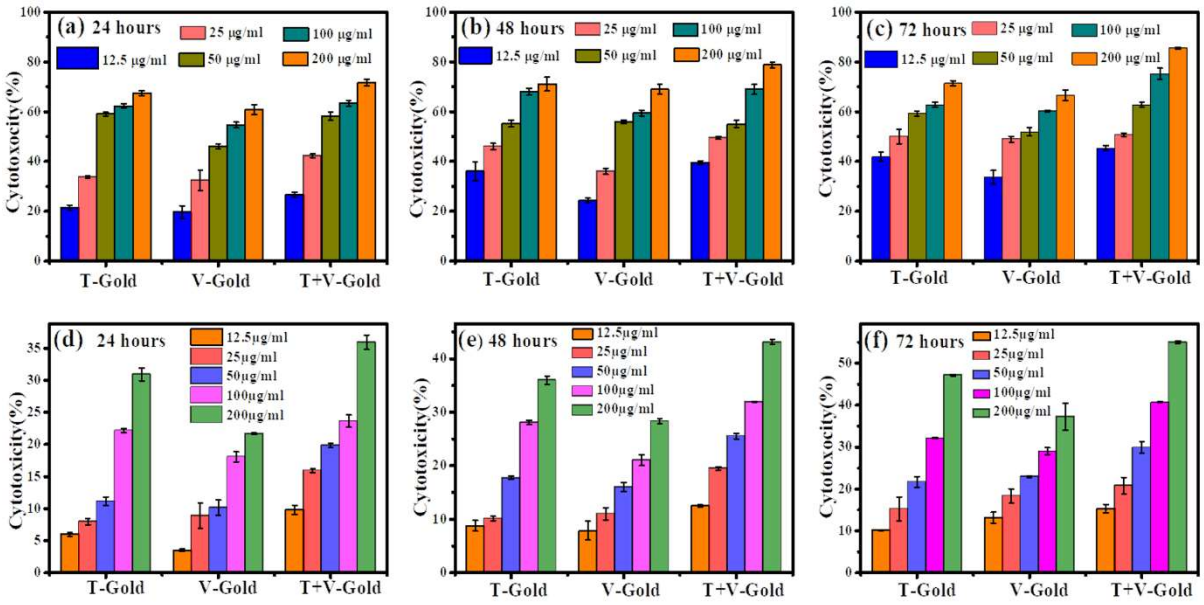

Figure 4. 5 Cytotoxicity and IC_{50} calculation of T-Gold, V-Gold, and T+V-Gold. (a-c) Dose dependent cytotoxicity assay of T-Gold, V-Gold, and T+V-Gold on 4T1 cells for 24hrs, 48hrs, and 72hrs. (d-f) Dose dependent cytotoxicity assay of T-Gold, V-Gold, and T+V-Gold on NIH-3T3 cells for 24hrs, 48hrs, and 72hrs.

4.2.6 Cellular Uptake Efficiency

The T-Gold, V-Gold, and T+V-Gold nanoparticles have a strong green fluorescence, that was easily studied by confocal microscopy when the NPs enter the 4T1 cancer cells. The 4T1 cells were exposed with the desired concentration of nano-formulation in RPMI medium at 37 ˚C for 2 and 4 hours before being observed. The nuclei were stained with DAPI for 20 minutes.

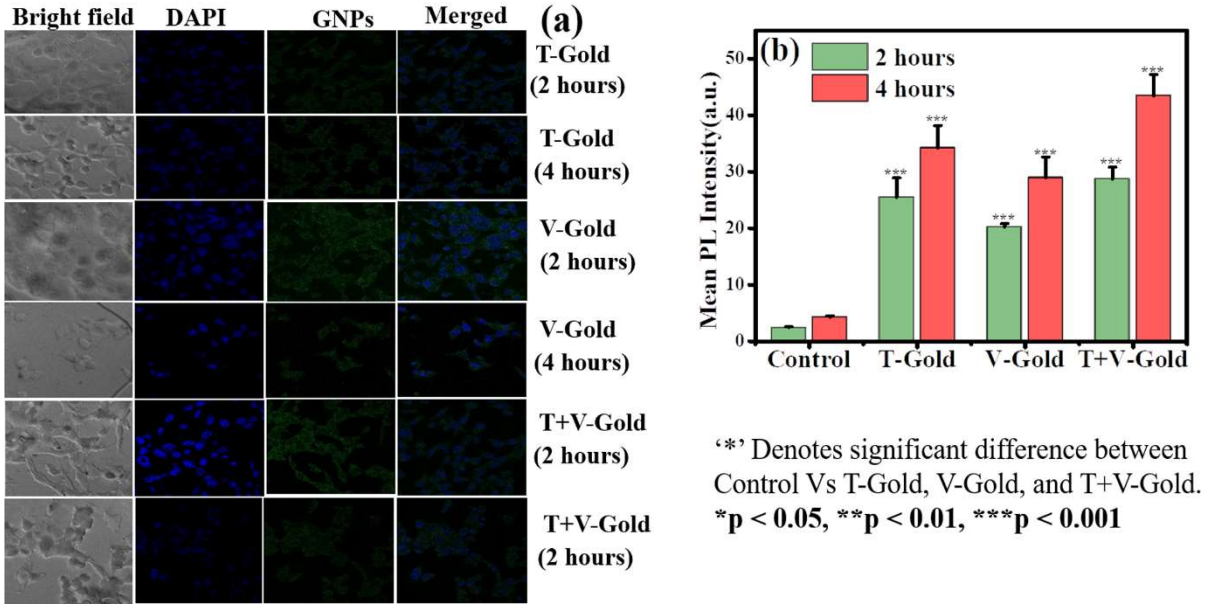

Figure 4. 6 (a) Confocal images of cellular uptake of T-Gold, V-Gold, and T+V-Gold by 4T1 metastatic breast cancer cells at different times after feeding T-Gold, V-Gold, and T+V-Gold, Blue is DAPI for labelling the nuclei, green emission from T-Gold, V-Gold, and T+V-Gold. (b) Quantification of the uptake using mean fluorescence intensity of T-Gold, V-Gold, and T+V-Gold in individual cells.

Figure 4.6(a) illustrates the green emission of NPs in the cytoplasm, suggesting that cancer cells can be able to internalise the NPs. As seen in Figure 4.6(b), the quantification of the uptake using mean fluorescence intensity (ImageJ) of nanoparticles increased over the course of the incubation period, depicting that 4T1 cells internalized the NPs.

4.2.7 Tumour Regression Study

From the seventh day after tumour induction until the day of sacrifice, the growth profile of 4T1 primary tumours in mice injected with T-Gold, V-Gold, and T+V-Gold started to relapse, as shown in Figure 4.7(a) and (c).

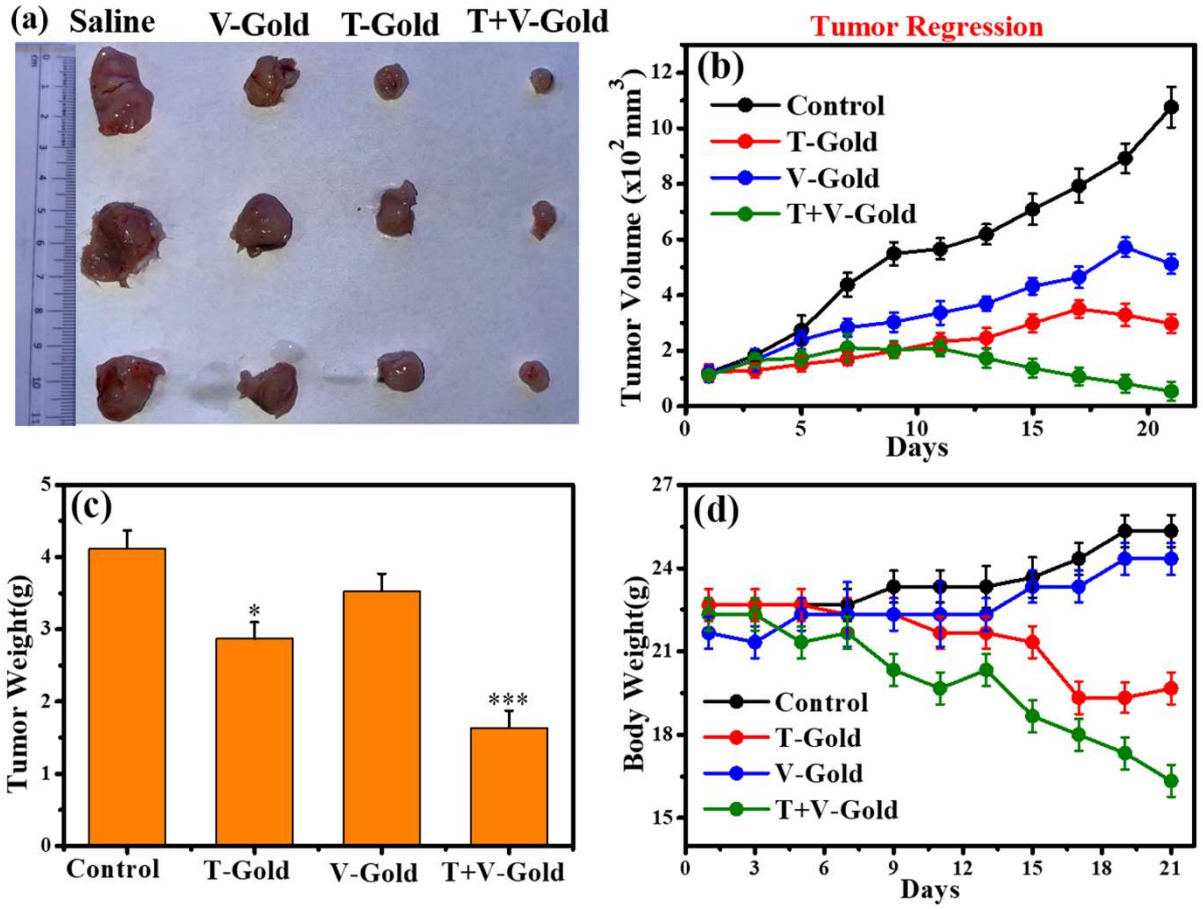

Figure 4. 7 The time period from tumour induction to the tumour regression in mice brought on by the nano-formulation (V-Gold, T-Gold and T+V-Gold). The BALB/c Model of 4T1 Mammary Carcinoma was developed, and the effects of IP injections of PBS (1X, pH 7.4), V-Gold (350mg/kg), T-Gold (350mg/kg), and T+V-Gold (350mg/kg) over the period of 21 days post-tumour induction were assessed. The mice were all sacrificed at the same time on day 21, the last day of the experiment. (a) the photograph of the mice's excised breast tumours at day 21 after tumour induction from four groups (n = 4 per group), (b) Graphical evolution of the tumour growth volume in treated mice (from day 10 days after tumour induction to day 21),

(c) Weight of excised tumour after treatment with the administered formulation, (d) Body weight of tumour-bearing mice during the course study.

'*' Denotes significant difference between Control Vs T-Gold and T+V-Gold.

***p<0.05, **p<0.01, ***p<0.001**

Interestingly, the effect of T+V-Gold on primary tumour volume was shown to be remarkable lower during the full-time course (up to a 3-fold reduction) in compared to PBS control, T-Gold and V-Gold groups (Figure 4.7(a) and (b)/Table 4.1(a)). In understanding with these results, when the weight of breast tumours excised at day 21 after tumour formation was compared between the V-Gold treated mice group and the PBS treated mice group, no significant differences were seen. However, it was demonstrated that the T+V-Gold group had a considerably lower tumour volume than the T-Gold treated group (Figure 4.7(c)/Table 4.1(b) and 4.7(d)/Table 4.1(c)).

(a)

T+V	T	V	Control	Days	Std. Control	Std. V	Std. T	Std. T+V
110.6015572	123.2784	116.9450663	121.3121047	1	30.13851	27.97032	26.95437	17.6075
166.3216523	128.196911	166.442643	183.3580493	3	23.07127	40.72241	25.55482	24.18848
173.695503	151.186617	238.931777	273.3847057	5	53.51084	33.95783	26.85272	27.11956
210.2438977	169.856084	283.4018773	437.771254	7	42.47417	31.96541	23.02132	49.05012
204.2039645	198.800556	302.5632943	548.810532	9	41.78179	34.63923	25.01419	28.8882
208.0572058	232.320834	336.2995178	566.2361387	11	37.89836	42.27083	30.75421	27.91253
172.6619203	245.585304	369.221966	618.5835252	13	36.8662	25.57638	36.76022	34.55916

137.6427433	298.872191	432.1109207	708.2597122	15	55.58266	29.81992	33.21017	34.61811
107.0432517	350.359213	463.9415833	793.111781	17	60.81991	38.54684	31.45444	21.69337
81.52905683	328.877663	572.1171527	891.9644507	19	53.52518	35.11439	40.49859	20.22177
53.64711267	297.053898	511.877504	1075.94082	21	72.58359	35.26868	33.14643	24.80187

(b)

	Tumor weight	**Std.**
Control	4.12	0.461628
V	3.526667	0.431895
T	2.87	0.226053
T+V	1.636667	0.366924

(c)

Groups					**Std.**			
T+V	**T**	**V**	**Control**	**Days**	**Control**	**V**	**T**	**T+V**
22.33333	22.6667	21.6667	22.66667	1	0.57735	0.57735	0.57735	0.57735
22.33333	22.66667	21.33333	22.66667	3	0.57735	0.57735	0.57735	0.57735
21.33333	22.66667	22.33333	22.66667	5	0.57735	0.57735	0.57735	0.57735
21.66667	22.33333	22.33333	22.66667	7	1.527525	1.154701	0.57735	0.57735
20.33333	22.3333	22.3333	23.33333	9	0.57735	0.57735	0.57735	0.57735
19.66667	21.66667	22.33333	23.33333	11	0.57735	1.154701	0.57735	0.57735
20.33333	21.66667	22.33333	23.33333	13	1.154701	0.57735	0.57735	1.527525
18.66667	21.33333	23.33333	23.66667	15	1.527525	0.57735	0.57735	0.57735
18	19.33333	23.33333	24.33333	17	1.154701	0.57735	2.886751	1
17.33333	19.33333	24.33333	25.33333	19	1.154701	0.57735	1.154701	0.57735
16.33333	19.66667	24.33333	25.33333	21	0.57735	0.57735	0.57735	0.57735

Table 4. 1 (a) Tumor Regression, (b) Tumor weight, (c) Body Weight Study of T, V, and T+V-Gold.

Importantly, the body weight of mice from the T+V-Gold treated group was significantly different from that of the untreated group. These data strongly indicate that T+V-Gold exhibited remarkable anti-breast tumour activity compared to T-Gold and V-Gold alone and saline groups. However, it induced mild toxicity-induced weight loss. Therefore, T+V-Gold may be a promising candidate for further development as an anticancer therapy.

4.2.8 Biochemical Estimations

The efficacy of tumour suppression after the administration of a manufactured formulation was evaluated by assessing oxidative stress and NO production using NO assay results. In the T-Gold and V-Gold treated group, the values for NO production in tumour tissue were 7.245±0.660 μM/mg and 5.580±1.434 μM/mg, respectively. However, in the T+V-Gold treated group, the values were increased to 7.795±2.344 μM/mg compared to the normal (2.570±0.669 μM/mg) as shown in Figure 4.8(a-c)/Table 4.2(a). LDH assay was used as a cellular biomarker for compromised cell membrane integrity, and the values for tumour tissue in the T-Gold treated group were 130.724±33.185 nM/mg. For tumour tissue in the V-Gold treated group, the values were 72.921±21.187 nM/mg. However, in the T+V-Gold treated group, the values were increased to 181.745±21.872 nM/mg compared to the normal (64.869±9.116 nM/mg), illustrated in Figure 4.8(d-f)/Table 4.2(b). The current oxidative stress-related assays demonstrate elevated levels of oxidative stress, which support the mechanism of tumour suppression in tumour-bearing animals after the administration of the different formulation. The concentration of SOD enzyme was investigated in tumour tissues under different conditions (Figure 4.8(g-i)/Table 4.2(c)). The study found that the concentration of SOD enzyme was 0.819±0.413 ng/mg in tumour tissue in the T+V-Gold treated group, while for

tumour tissue in the T-Gold treated group and tumour tissue in the V-Gold treated group, the values were 1.346±0.810 ng/mg and 1.239±0.091 ng/mg, respectively. These values were further compared to a normal control group where the concentration of SOD enzyme was found to be 2.932±0.167 ng/mg, shown in Figure 4.8(i).

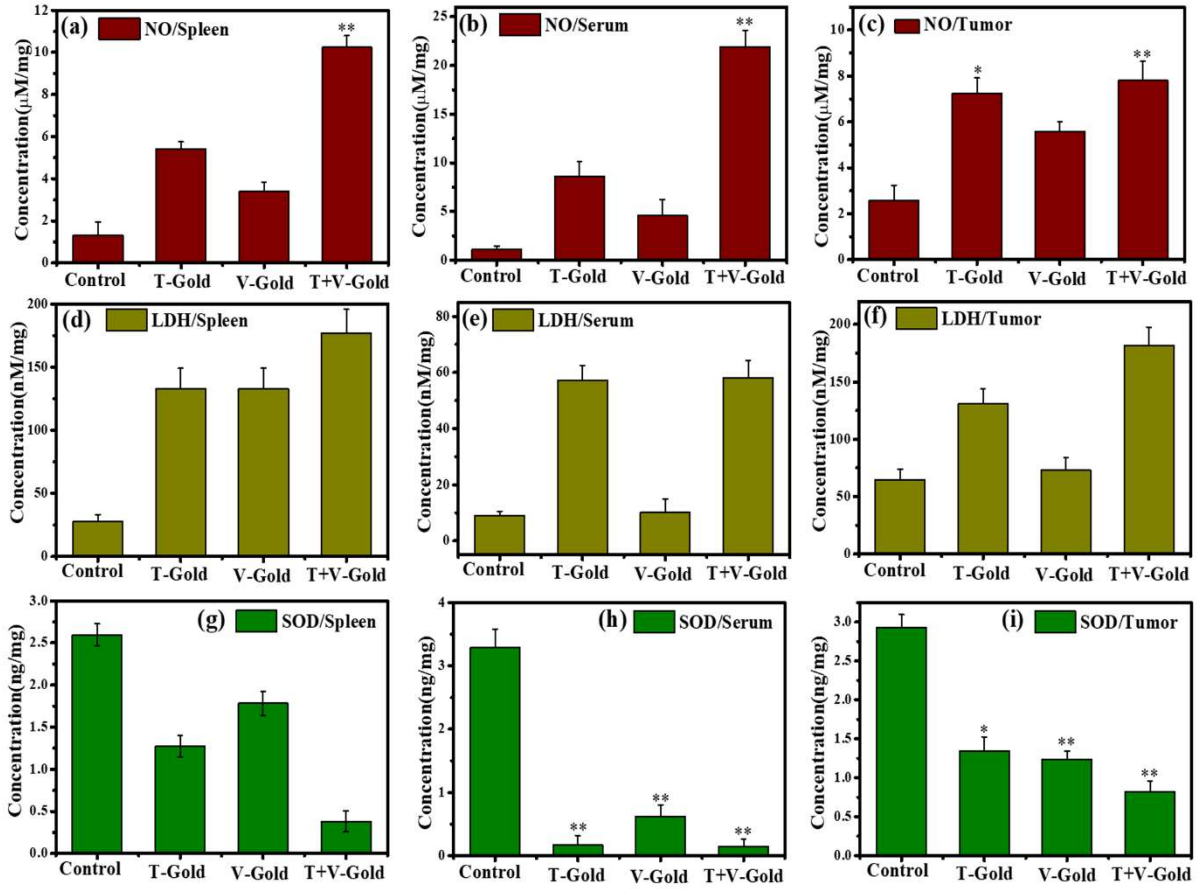

Figure 4. 8 (a-c) NO level, (d-f) LDH level, (g-i) SOD level in 4T1 treated mice.

'*' Denotes significant difference between Control Vs T-Gold and T+V-Gold.

***p<0.05, **p<0.01, ***p<0.001**

(a)

NO assay			
Groups	**Spleen**	**Serum**	**Tumor**
control	1.314±0.626	1.102±0.366	2.570±0.669
V	3.404±0.433	4.601±1.930	5.580±1.434
T	5.427±0.329	8.599±3.558	7.245±0.660
T+V	10.248±3.548	21.879±7.721	7.795±2.344

(b)

LDH assay			
Groups	**Spleen**	**Serum**	**Tumor**
control	27.443±5.702	9.081±0.459	64.869±9.116
V	132.799±56.534	10.040±4.855	72.921±21.187
T	133.036±50.898	57.252±11.362	130.724±33.185
T+V	177.022±43.728	58.147±19.201	181.745±21.872

(c)

SOD assay			
Groups	**Spleen**	**Serum**	**Tumor**
control	2.595±0.320	3.288±1.295	2.932±0.167
V	1.782±0.867	0.620±0.184	1.239±0.091
T	1.273±0.003	0.167±0.154	1.346±0.810
T+V	0.381±0.023	0.147±0.113	0.819±0.413

Table 4. 2 (a) NO assay, (b) LDH assay, (c) SOD assay data for oxidative stress are represented as mean± stdev with n=4, in different tissue samples.

In the study, the concentration of glutathione (GSH) was measured in tumour tissue samples from different groups of treated subjects. The group that received T+V-Gold treatment showed a GSH concentration of 1.815±0.160 nM/mg, which was significantly lower than the normal control group (4.275±2.098 nM/mg). The tumour tissue samples from the T-Gold treated group and V-Gold treated group showed GSH concentrations of 2.446±1.495 nM/mg and 2.610±0.485 nM/mg, respectively, shown in Figure 4.9(a-c)/Table 4.3(a)[235], [236].

Additionally, the GST assay was performed on tumour tissue samples from these groups, and the results showed that the GSH transferase (GST) activity in the tumour tissue samples from the T-Gold treated group was 92.126±14.174 nM/mg, while in the V-Gold treated group, it was 63.848±10.892 nM/mg. The T+V-Gold treated group showed a significant increase in GST activity, with a value of 180.410±8.868 nM/mg, compared to the normal control group (27.004±5.438 nM/mg), illustrated in Figure 4.9(d-f)/Table 4.3(b).

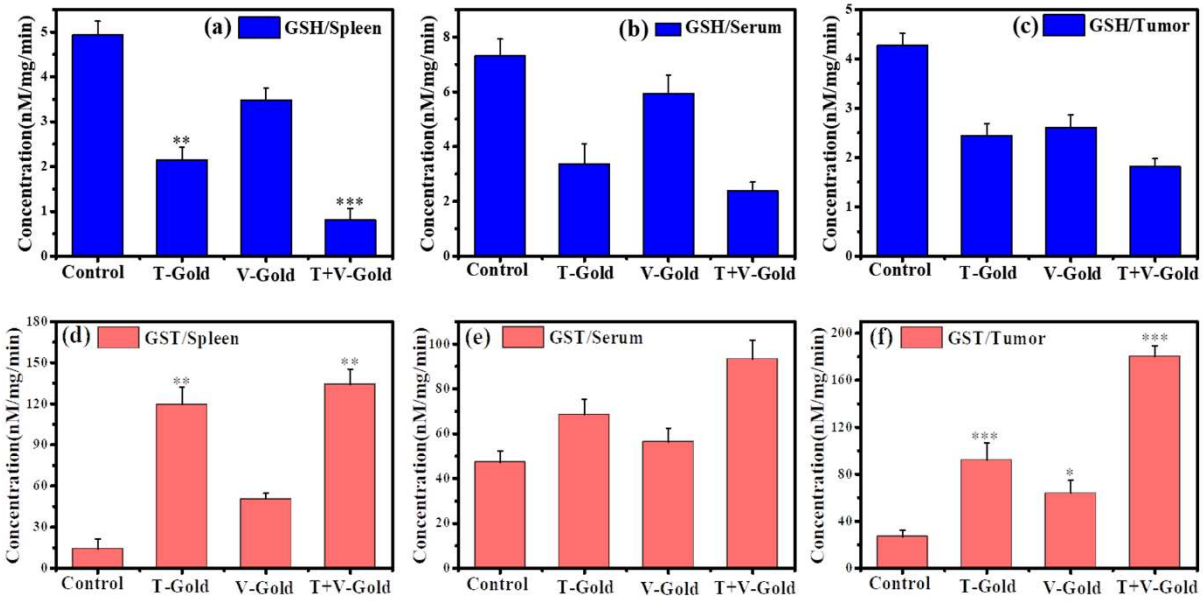

Figure 4. 9 (a-c) GSH level, (d-f) GST level in 4T1 treated mice.

'*' Denotes significant difference between Control Vs T-Gold and T+V-Gold.

***p<0.05, **p<0.01, ***p<0.001**

(a)

GSH assay			
Groups	**Spleen**	**Serum**	**Tumor**
control	4.940±0.981	7.326±0.595	4.275±2.098
V	3.485±0.657	5.936±3.667	2.610±0.485
T	2.150±0.826	3.370±1.732	2.446±1.495
T+V	0.818±0.483	2.396±0.306	1.815±0.160

(b)

GST assay			
Groups	**Spleen**	**Serum**	**Tumor**
control	14.148±8.950	47.304±15.057	27.004±5.438
V	50.540±4.078	56.323±15.977	63.848±10.892
T	119.520±25.528	68.543±33.790	92.126±14.174
T+V	134.178±38.117	93.284±34.376	180.410±8.868

Table 4. 3 (a-c) GSH level, (d-f) GST level in 4T1 treated mice.

'*' Denotes significant difference between Control Vs T-Gold and T+V-Gold.

***p<0.05, **p<0.01, ***p<0.001**

4.3 Discussion

The present study investigated the synthesis of gold nanoparticles using Tulsi and *Vinca* extracts, labelled as T-Gold, V-Gold, and T+V-Gold, respectively. The synthesized nanoparticles were characterized using transmission electron microscopy (TEM) and selective area electron diffraction (SAED) pattern analysis, as shown in Figure 4.1(a-c). The TEM images showed that T-Gold had large particle sizes with different shapes, while V-Gold had small particle sizes but a mixed phase. The T+V-Gold nanoparticles exhibited a medium range of particle sizes with different shapes. The SAED pattern analysis revealed that all synthesized nanoparticles were crystalline in nature with a small amount of amorphous phase. SAED pattern analysis provided valuable information about the crystallographic nature of the synthesized nanoparticles. Overall, these findings suggest that both Tulsi and *Vinca* extracts can be used for the synthesis of gold nanoparticles with different size and shape characteristics. Figure 4.1(e) shows the emission spectra of T-Gold, V-Gold, and T+V-Gold synthesized materials. It was observed that the maximum emission of T-Gold, V-Gold, and T+V-Gold occurred at 410 nm, 440 nm, and 450 nm, respectively, at a concentration of 0.23 μg/ml and an excitation wavelength of 280 nm. It was found that the emission intensity was significantly high in T+V-Gold synthesized materials compared to T-Gold and V-Gold. the colloidal solution contained particles of varying sizes in XRD, a broad peak at 2Θ = 25 was also observed, indicating the presence of a small amount of amorphous phase, which was attributed to the plant extract used in the synthesis process. The most intense peak at 2Θ = 38.1 in the XRD pattern for T+V gold further revealed that the synthesis of gold nanoparticles with T+V-Gold was superior to that of T-Gold and V-Gold. The intense diffraction observed at the 38.1 larger diameters exhibiting most of the intensity peak indicated that the preferred growth orientation of the zero valent gold was fixed in the (111) direction. This characteristic pattern

was typical of pure gold nanoparticles[237]. However, a small amount of amorphous nature (crystalline impurity) occurring due to the surface functionalization of mediational plant extract on GNPs. In the green synthesis method, occurrence of crystalline impurities can be attributed to various factors like reduction agent and stabilizing agent, reaction conditions, purity of starting materials, contamination of solvents, incomplete of reaction, purification and many more factor affecting the crystallinity growth during the reaction[55], [238]. The measured zeta potential values for T-Gold, V-Gold, and T+V-Gold were -28.5 mV, -22.3 mV, and -32.4 mV, respectively, as shown in Figure 4.1(g). These values confirm the stability of the synthesized colloidal stock solution of GNPs. To determine the distribution of hydrodynamic diameters of the GNPs in the T-Gold, V-Gold, and T+V-Gold samples, dynamic light scattering (DLS) was used. Figure 4.1(h) shows that the broad peak in dynamic light scattering (DLS) measurements typically arises due to the presence of particles with a wide range of sizes or the coexistence of multiple populations of particles in the synthesized samples.

FTIR results demonstrate that T-Gold, V-Gold, and T+V-Gold are decorated with various functional groups, including nitrogen, oxygen, and carbon atoms. The high concentration of oxygen-containing functional groups presents on GNPs surfaces make them highly soluble in water. These findings suggest that T-Gold, V-Gold, and T+V-Gold possess excellent solubility characteristics in aqueous solutions, which can be attributed to the presence of various functional groups on their surfaces. The C1s, O1s, N1s, and Au 4f deconvolution spectra of T-Gold, V-Gold, and T+V-Gold were analysed to identify the various functional groups present in the synthesized gold nanoparticles, shown in Figure 4.2(a-i).

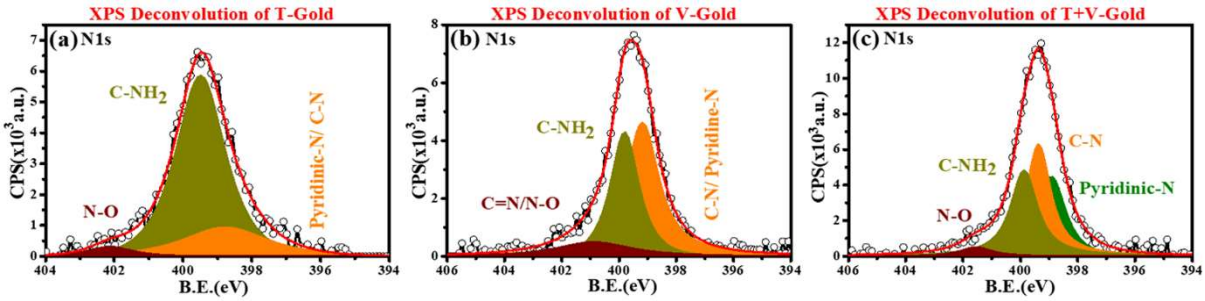

Figure 4. 10 Deconvolution of N1s photoelectron XPS spectrum. (a) T-Gold, (b) V-Gold, and (c) T+V-Gold samples.

The C1s peak was deconvoluted to reveal the presence of C=O, C-N/C-O, and C-C/C=C functional groups at approximate positions of 287.82, 285.82, and 284.24 eV, respectively[55], [239]. The O1s peak was deconvoluted to identify C-OH/O-C=O, C-O/C=O, and O-O functional groups at approximate positions of 532.67, 531.99, and 530.69 eV, respectively[240]. The Au 4f deconvolution spectrum showed the presence of $4f_{7/2}$ (Au^o) and $4f_{5/2}$ (Au^o) peaks in T-Gold, V-Gold, and T+V-Gold at approximately 83.3 eV, and 87.1 eV, respectively[241], [242]. The N1s deconvolution spectrum of T-Gold, V-Gold, and T+V-Gold revealed the presence of N-O, C-NH_2, and C-N/pyridinic-N functional groups at approximately 399.15, 399.78, and 398.47 eV, (Figure 4.10) respectively. The atomic percentages of C1s, O1s, N1s, and Au 4f were determined for each sample, and it was found that the highest percentage of gold synthesis was achieved in T+V-Gold, illustrated in Table 4.4(a). The position and area percentages of various functional group species in T-Gold, V-Gold, and T+V-Gold were also calculated and are presented in Table 4.4(b).

(a)	**T-Gold**		**V-Gold**		**T+V-Gold**	
	Range	**Atomic%**	**Range**	**Atomic%**	**Range**	**Atomic%**
C1s	291-279	67.39	294-277	71.03	293-279	66.16

O1s	538-523	27.06	538-523	25.12	537-523	25.11
N1s	408-394	2.7	409-392	3.08	403-390	4.53
Au4f	91-77	2.85	92-81	0.77	92-77	**3.54**

(b)	**Functional Groups**	**T-Gold**		**V-Gold**		**T+V-Gold**	
		Position	**Area%**	**Position**	**Area%**	**Position**	**Area%**
C1s	**C-C/C=C**	284.24	64.69	284.40	64.54	284.24	59.26
	C-N/C-O	285.82	25.70	285.92	26.41	285.74	28.13
	C=O	287.83	9.61	287.92	9.06	287.65	12.61
O1s	**C-OH/O-C=O**	532.67	33.17	532.70	35.27	532.57	31.58
	C-O/C=O	531.99	56.84	532.00	47.39	531.99	38.94
	O-O	**530.69**	**9.90**	**530.82**	**16.58**	**531.29**	**29.48**
Au 4f	**4f7/2(Au^o)**	83.35	43.17	83.20	38.37	83.43	38.41
	Au^+	83.30	13.59	83.38	16.38	83.32	15.34
	4f5/2(Au^o)	87.04	32.44	87.13	12.66	87.10	33.57
	Au^+	86.84	10.80	86.88	32.59	86.80	12.68

Table 4. 4 (a) Atomic percentage of C1s, O1s, N1s, and Au 4f of T-Gold, V-Gold, and T+V-Gold, (b) Area% of functional groups present in C1s, O1s, N1s, and Au4f of T-Gold, V-Gold, and T+V-Gold.

The presence of these functionalized gold nanoparticles can lead to the development of unique optical and biological characteristics, which may have potential applications in antioxidant and anticancer activities. The presence of antioxidants can cause a change in color from purple to yellow in the DPPH assay, as the nitrogen-containing free radicals are converted into stable neutral DPPH-H complexes after accepting hydrogen ions, as illustrated in inset Figure 4.4(a), (d), and (g). Previous research has also reported on the DPPH scavenging activity of

nanoparticles[243]. In this study, T-Gold, V-Gold, and T+V-Gold nanoparticles demonstrated excellent DPPH scavenging potential, as shown in Figure 4.4(b), (e), and (h). The IC_{50} values obtained for T-Gold, V-Gold, and T+V-Gold were 0.241 µg/mL, 0.352 µg/mL, and 0.180 µg/mL, respectively (Figure 4.4(c), (f), and (i)). T+V-Gold exhibited the lowest IC_{50} value, indicating a higher availability of unpaired electrons, a higher surface-to-volume ratio, and the presence of surface defects, making them more sensitive to scavenging free radicals at lower concentrations[244].

Moreover, T-Gold exhibited faster cytotoxicity (~24 hours) than V-Gold (~48 hours). These findings are consistent with previous studies scrutinized by Gautam et al. and Ke et al., which reported the cytotoxicity of T-Gold and V-Gold, respectively against cancer cells[235], [245]. The results showed that exposure to the various concentrations of GNPs formulation resulted in a dose-dependent manner to inhibit the growth of 4T1 cells (Figure 4.5(a-c)) and NIH-3T3 cells (Figure 4.5(d-f)). After exposure to the various multiple modalities to NIH-3T3 showed negligible cytotoxicity in compared to 4T1 cells. Therefore, the most commonly used mitotic inhibitor paclitaxel and Mitomycin-c reported to exhibited off target effect by inhibiting the activity of normal cells and cancer cells[246]. The demonstrates the individual drugs concentration-dependent cytotoxicity on 4T1 cells, with T-Gold exhibiting more potent inhibition of cell growth (IC_{50} = 83.11708 µg/ml) than V-Gold (IC_{50} =115.4755 µg/ml). The combined effect of T+V-Gold suspension on cancer cells was evaluated. The results showed that the percentage cytotoxicity was drastically enhanced in the case of T+V-Gold nano-formulation with lower IC_{50} values of 10.29603 µg/ml, 34.35572 µg/ml, and 65.39164 µg/ml for post-72 hours, 48 hours, and 24 hours, respectively Figure 4.5(a-c)/Table 4.5. The slightly lower cell cytotoxicity observed for V-Gold at most concentrations compared to the bare T-Gold was also noted. The enhanced cytotoxicity of T+V-Gold was probably due to the

increased bioavailability and combination effects of the formulation. It caused enhanced permeation through the cell wall to indicate its anti-cancer metabolites were quickly released and reach cell organelles and thereby exhibiting cell death. Survey of the available literature suggested that the bio-fabrication of dual systems induced enhanced anti-cancer efficacy against various cancers[247]. On the other hand, Paclitaxel and mitomycin-C exhibited potent anti-cancer effect were used as positive control in various studies demonstrated dose dependent cytotoxicity similarly to T-Gold, V-Gold and T+V gold (Figure 4.11(a))[248]. The IC_{50} value found corresponding to Paclitaxel as 22.2 µg/ml (Table 4.5).

Time (hours)	IC_{50} Dose (µg/ml)			
	T-Gold	**V-Gold**	**T+V-Gold**	**Paclitaxel**
72	25.50671	61.20838	10.29603	-
48	46.17703	82.46611	34.35572	-
24	83.11708	115.4755	65.39164	22.2

Table 4. 5 Containing IC_{50} dose of T-Gold, V-Gold, T+V-Gold, and Paclitaxel against 4T1 metastatic breast cancer.

These findings suggest that T+V-Gold may have potential as a therapeutic agent for breast cancer treatment. Overall, this study provides valuable insights into the cytotoxicity effects of T-Gold, V-Gold, T+V-Gold, and Paclitaxel their potential applications in cancer therapy.

The maximum fluorescence intensity was observed in T+V-gold treated groups in compared to individual T and V-gold within 2 and 4 hours of incubation shown in Figure 4.6(b). These findings suggest that GNPs have the potential as efficient carriers for anti-cancer agents, and their small size enables them to cross the cell membrane and reach the tumour cells. The use

of fluorescent GNPs allows for visualization and tracking of their cellular uptake, which can aid in the advancement of targeted and operative cancer therapies. Innumerable studies have reported the antitumour activity of T-Gold and V-Gold nano-formulations both *in vitro* and *in vivo*[249]. However, the chemo-preventive and anti-tumour effects of T+V-Gold nano-formulation have not been well explored *in vivo* study. To investigate this, we used a dose of 34.35572 μg/ml of T+V-Gold nano-formulation, which was the IC_{50} dose for 48 hours, for all *in vivo* experiments. We treated 4T1 tumour-challenged mice with T-Gold, V-Gold and T+V-Gold nano-formulations, and found that all three formulations resulted in delayed tumour development and lower tumour burden in a dose-dependent manner (Figure 4.7). Interestingly, T+V-Gold nano-formulation demonstrated the highest reduction, delaying the formation of tumour compared to the untreated 4T1-challenged mice in the saline group (Figure 4.7(a)). This is due to presence of vincristine and vinblastine derived from Vinca and eugenol, rosmarinic acid, and apigenin extracted from Tulsi leaves-exhibited potent anti-cancer activity[215]–[218], [250] similar manner to chemotherapeutic mitotic drugs-paclitaxel and mitocmycin-c. Our findings suggest that T+V-Gold nano-formulation may have potential chemo-preventive and anti-tumour effects in metastatic breast cancer. To investigate the overall oxidant mechanisms in cancer and the effect of T-Gold, V-Gold, and T+V-Gold NPs on reducing tumour burden, we have investigated various glutathione family antioxidants such as GST, GSH, as well as SOD in serum on the 21st day of the experiment[245], [251]. The oxidative stress of a cell is a state in which ROS production rises or the amount of scavenged ROS falls in cells. There is evidence that oxidative stress has a role in the pathogenesis of cancer[252]. Additionally, ROS are produced following by chemotherapy and radiotherapy, as well as upon exposure to physical agents like heat and UV light. These ROS can act as defence mechanisms against tumour burden. Overall, understanding the role of ROS in cancer and developing strategies to manipulate ROS levels may offer potential therapeutic targets for

cancer treatment. The presence of nitric oxide (NO) and LDH in a tumour-specific state is a biomarker for oxidative stress. In the tumour microenvironment, the two distinct isoenzymes for NO synthase, iNOS and nNOS, catalyze the conversion of L-arginine to L-citrulline in an oxygen and NADPH-dependent process, supporting NO production. iNOS is primarily used as a measure of NO generation in an inflammatory milieu around[253]. The liver plays various roles within the body that are vital for a healthy life. GNPs exposure can cause oxidative stress in hepatic tissues via different mechanisms. Exposure to GNPs can cause their accumulation in the liver, consequently disturbing the activities of antioxidant enzymes and causing oxidative stress in the liver. In liver, control and GNPs-injected mice exhibited minimal lesions, corresponding to normal liver. All the three nanoparticles showed negligible toxicity. A complete description of the histopathological findings is showed in Figure 4.11(b)[254].

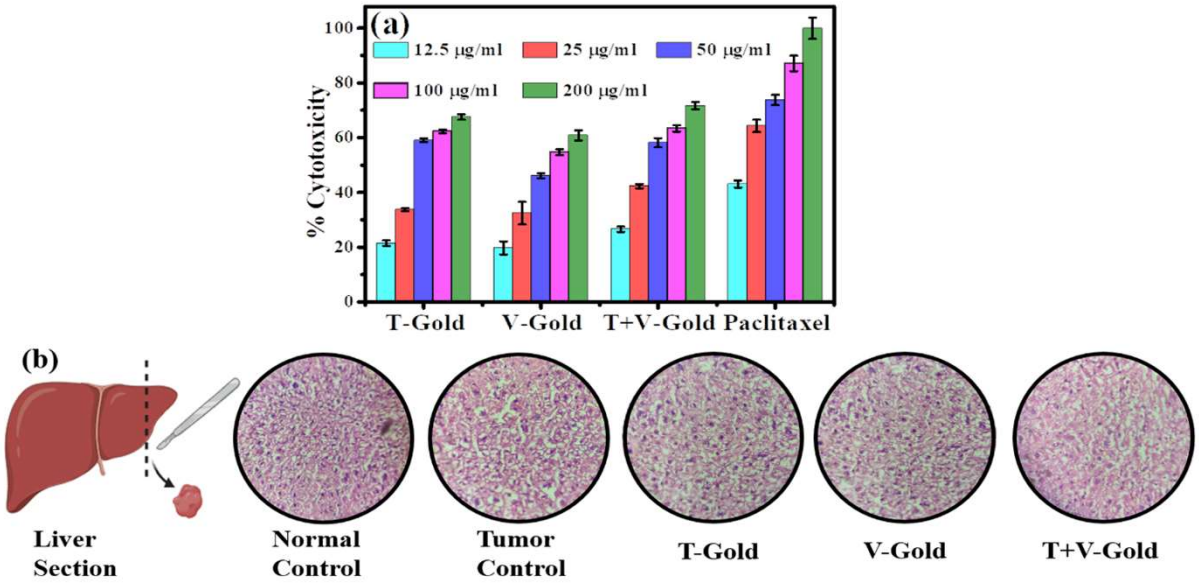

Figure 4. 11 (a) Dose dependent cytotoxicity of T-Gold, V-Gold, T+V-Gold, and Paclitaxel, (b) Histopathology of the liver section at magnification 40X. Light micrographs of the liver sections from different treatment groups. Normal Control mouse liver section showing normal

hepatic architecture of binucleated cells and activated Kupffer cells. The Tumor control, T, V and T+V group didn't show any pathological remarks related to lesions, steatosis and the abundance of micro and macro vesicles in compared to normal control. All the groups showed binucleated cells refer to regeneration.

Superoxide dismutase (SOD) is an enzyme that acts as a potent antioxidant defence mechanism by catalysing the dismutation of superoxide anion (O^-), a potent oxidant and nitro sating agent that can cause direct damage to proteins, lipids, and DNA. Our SOD results suggest that the concentration of SOD enzyme was lower in tumour tissues under different conditions compared to normal tissues, indicating a potential role of SOD in preventing oxidative damage in tumours. The T+V-Gold treatment may have a positive effect on the GST activity in tumour tissue samples, which could potentially help to reduce the risk of cancer progression. Gold and silver nanoparticles have been explored in generation of ROS in cancer cells, which can lead to apoptosis[255], [256]. In a study, it was observed that the level of ROS generation was significantly higher in the T+V group compared to the T-Gold and V-Gold nano-formulations alone. This was reflected by the increased levels of NO, GST, LDH, GSH, and SOD, which are responsible for oxidative damage. The elevated levels of ROS generation in the T+V group suggest that the combined effect of the T and V nano-formulations have remarkable anticancer activity compared to the individual formulation. This may be due to the synergistic effect of the two formulations, which enhances their ability to induce ROS generation and subsequent apoptosis in cancer cells. However, further studies are needed to elucidate the exact mechanisms underlying this effect and to evaluate the safety and efficacy of the T+V formulation in preclinical and clinical trials.

4.4 Conclusion

In the present work, we have synthesized gold nanoparticles (GNPs) using extracts of Tulsi and *Vinca*. The mixed of Tulsi and *Vinca* extract for GNPs caused significant breast cancer tumour regression in mice model. The physical properties were evaluated using UV-VIS, TEM, XRD, PL, FTIR, XPS, Zeta and DLS. The synthesized GNPs have different shapes and sizes with higher crystallinity. The GNPs also have emitting properties ranging from blue to green at 280 nm excitation and absorb light at 280 nm and 555±15 nm. FTIR and XPS confirmed the presence of the different functional groups on the surface of the synthesized GNPs. These decorated GNPs showed that the zeta potential values for T-gold, V-gold and T+V-gold were -28.5 mV, -22.3 mV and -32.4 mV, respectively. The broad peak in the dynamic light scattering (DLS) measurements typically arises from the presence of particles with a broad size spectrum or the coexistence of multiple populations of particles in the synthesized samples. The inhibitory effects of T-Gold, V-Gold, and T+V-Gold on the growth of 4T1 cells were evaluated using the MTT assay. The combination of T+V-Gold exhibited higher cytotoxicity compared to bare T-Gold and V-Gold, which resulted in the rapid release of anti-cancer metabolites that easily reached the cell organelles, thereby exhibiting cytotoxicity but also showed less cytotoxicity on NIH-3T3 cells. In liver, control and GNPs injected mice exhibited minimal lesions, corresponding to normal liver. T-Gold, V-Gold, and T+V-Gold showed negligible toxicity. T+V-Gold nano-formulation demonstrated the better regression of tumour when compared to the untreated 4T1-tumour bearing mice treated with PBS. To understand the underlying mechanism of the reduced tumour burden post treatment with T-Gold, V-Gold, and T+V-Gold NPs, the anti-oxidant pathways altered in cancer, such as glutathione family including GST, GSH, as well as SOD in serum. NO and LDH showed increased oxidative stress that was well supported by the mechanism of tumour suppression in tumour-bearing animals after the administration of the formulation. The concentration of SOD enzyme was

lower in tumour tissues under different conditions compared to normal tissues, indicating a potential role of SOD in preventing oxidative damage in tumours. The T+V-Gold treatment may have a positive effect on the GSH and GST activity in tumour tissue samples, which could potentially help reduce the risk of cancer progression. In summary, the T-Gold, V-Gold, and T+V-Gold nanoparticles demonstrated good stability, DPPH scavenging potential, cytotoxicity, and in vivo anti-cancer potential in 4T1 tumour bearing mice.